

BS24

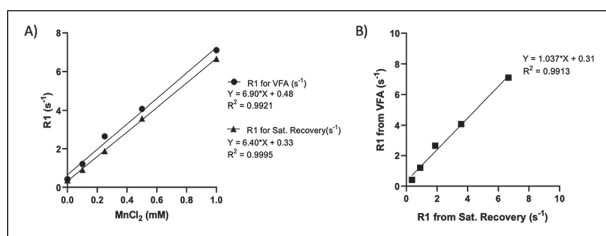
# T1 MAPPING IN A MOUSE MODEL OF MYOCARDIAL INFARCTION MODEL USING VARIABLE FLIP ANGLE MANGANESE ENHANCED MRI

<sup>1</sup>Shahrani Janudin, <sup>2</sup>Zhiping Feng, <sup>2</sup>Daniele Tolomeo, <sup>3</sup>Mark Lythgoe, <sup>2</sup>Jack Wells, <sup>2</sup>Daniel Stuckey. <sup>1</sup>Centre for Advanced Biomedical Imaging, UCL, London; Faculty of Health Science, UiTM, Malaysia, Centre for Advanced Biomedical Imaging Paul O' Gorman Building, UCL London, LND WC1E6DD UK; <sup>2</sup>Centre for Advanced Biomedical Imaging, UCL, London; <sup>3</sup>Advanced Biomedical Imaging, UCL, London

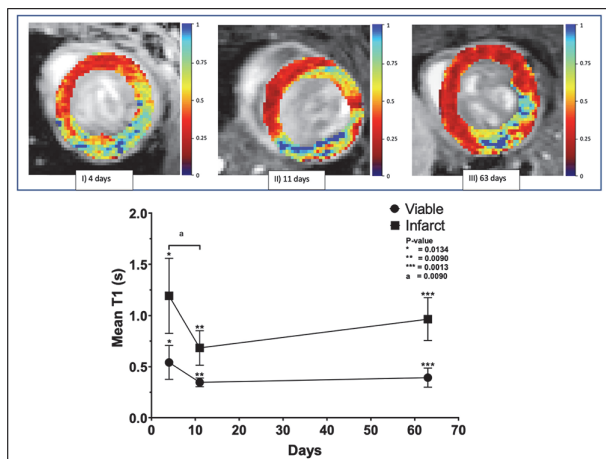
10.1136/heartjnl-2022-BCS.204

**Introduction** T1 mapping is a quantitative MRI approach that calculates the longitudinal relaxation time of the tissue based on the signal amplitude in different T1 weighted images<sup>1</sup>. Manganese is a clinically relevant T1 contrast medium that enters myocytes via active calcium channels, thereby lowering T1 in viable myocardium<sup>2 3</sup>. The Lock-looker inversion recovery sequence is the standard method for T1 measurements. However, there are limitations to this technique including long acquisition times and inconsistent T1 estimates. Here we use a Variable Flip Angle (VFA) approach and manganese enhanced MRI (ME MRI) to measure T1 changes post myocardial infarction in mice.

**Methods** The VFA T1 mapping approach was first validated against phantom samples in vitro. Myocardial infarction was then induced in 6 C57BL/6 female mice. ME MRI was performed 4 days, 11 days, and 63 days after infarction using a 9.4T Bruker system. Bright blood imaging was acquired 30 min after 0.1mmol/kg i.p. MnCl<sub>2</sub> using a 3D Intragate (IG)



**Abstract BS24 Figure 1** Figure 1(A): In vitro graph of longitudinal relaxation rate constant (R1) in different MnCl<sub>2</sub> concentration (mM) for VFA and saturation recovery. (B) R1 from VFA versus R1 from saturation recovery.



**Abstract BS24 Figure 2** Figure 2) ME MRI T1 maps acquired at 4, 11 and 63 days post myocardial infarction and mean T1 measurements from the infarct region and the viable myocardium over 63 days.

FLASH protocol at flip angles of 2°, 8°, and 14°, with TR/TE=10ms/1.8ms, slab thickness=5mm, FOV=25mm x 25mm, matrix size =128x128x10, bandwidth=98684.2kHz, navigator slice: pulse= 2°, thickness=3mm, bandwidth: 1826.7kHz were used. T1 was estimated using the DESPOT1 protocol.

**Results** The VFA approach gave similar longitudinal relaxation rates (R1=1/T1) to those acquired using an established saturation recovery method in a manganese phantom containing 0mM, 0.1mM, 0.2mM, 0.5mM and 1.0mM MnCl<sub>2</sub> (Figure 1A & B). ME MRI of the infarcted tissue gave higher T1 values than the remote myocardium at all time points as the damaged tissue was unable to uptake manganese (Figure 2). Infarct ME MRI T1 was higher on day 4 than day 11 (P=0.012) which may be due to post infarct inflammatory cell infiltration and oedema facilitating manganese accumulation.

**Conclusion** The VFA approach can rapidly and accurately measure T1 and when combined with manganese injections can be used to identify the infarcted regions of the myocardium.

BS25

# HUMAN MACROPHAGES ARE IMMUNOPROFILED BY PERICARDIAL FLUID SMALL EXTRACELLULAR VESICLES MODULATING LIPID METABOLISM MECHANISMS

<sup>1</sup>Soumaya Ben-Aicha, <sup>2</sup>Maryam Anwar, <sup>2</sup>Prakash Punjabi, <sup>3</sup>Jacques Behmoaras, <sup>2</sup>Costanza Emanuelli. <sup>1</sup>Imperial College London, Du cane Road London, LND W12 0NN UK; <sup>2</sup>Imperial College London; <sup>3</sup>Duke-NUS Medical School

10.1136/heartjnl-2022-BCS.205

**Background** The incidence and severity of ischemic heart disease (IHD) is exacerbated by coronary artery disease (CAD). Monocytes and macrophages are central to atherosclerosis. Endogenous small extracellular vesicles (sEVs) can shuttle microRNAs and other molecular cargos from cell to cell, mediating expressional and functional response in the recipient cells. Recent evidence supports a role for sEVs in modulating macrophage phenotype. The pericardial fluid (PF) is in direct contact with the epicardium and contain sEVs. We recently showed that human PF-sEVs are capable to modulate cardiovascular cells via microRNA shuttling (C.Beltrami et al.2017).

**Purpose** This study sought to investigate whether PF-sEVs regulate macrophages, contributing to a specific immunophenotype in CAD patients.

**Methods** PF was collected from either CAD patients undergoing coronary bypass surgery (CABG) or non-atherosclerotic patients operated for mitral valve repair (non-CAD control group). sEVs were isolated using size exclusion chromatography and characterised for size (Nanosight tracking analysis; NTA), tetraspanin content (by Nanoview chips), microRNA content by RNA seq and proteomic analysis. Monocytes from healthy donors were isolated from buffy coats and differentiated into macrophages following established protocols. Macrophages were incubated with either CAD-sEVs or non-CAD sEVs for 24h at 37°C. The cells were collected and processed for mRNA analyses (qRT-PCR) and flow cytometry. Human PF-cells were isolated and analysed to be compared with the in vitro setting. Further bioinformatics were employed to understand functional pathways and validated in PF from patients.

**Results** Exposure to CAD-sEVs induces a proinflammatory profile of human macrophages. CAD-sEVs treated macrophages showed a CD36+low, CD206+low CD40+high

profile. While non-CAD-sEVs did not statistically differ from PBS nor untouched groups, CAD-sEVs increased the mRNA level of IL1a, IL1b, TNFa and decreased MRC1. Proteomics revealed that PF-sEVs from CAD patients carried higher amounts of pro-inflammatory molecules (ICAM-1 and IL18) compared to NonCAD control. Bioinformatics analysis showed that 861 miRNAs were decreased in the PF-sEVs from CAD patients compared to non-CAD. miRNA targets prediction and pathway analyses reported that clusters of deregulated miRNAs could regulate CD36 and SRB1 which were shown to be decreased in CAD-sEVs treated macrophages. Human PF-cells revealed a reduced expression of CD36 on PF-macrophages.

**Conclusions** We demonstrate, for the first time, that sEVs isolated from the PF of CAD patients induce a proinflammatory profile of human macrophages and that target crucial lipid metabolism pathways. These clinically relevant results could drive to decipher improved therapeutics able to modulate the epicardial/myocardial immune response in CAD patients.

## BS26 ROLE OF KMT2C, A HISTONE METHYLTRANSFERASE IN THE DEVELOPMENT OF COMPACTED MYOCARDIUM

Sabu Abraham. University of Manchester, Core Technology Facility, 46 Grafton Street, Manchester, GTM M13 9NT UK

10.1136/heartjnl-2022-BCS.206

Epigenetic gene regulation has been increasingly established as a pivotal molecular mechanism driving heart development and its aberrant regulation has been implicated in congenital heart diseases. KMT2C is a histone methyltransferase enzyme that mediates the Histone 3 lysine 4 (H3K4) methylation that denotes active promoters and enhancers. Our previous work identified a number of de novo variants in KMT2C gene in nonsyndromic Tetralogy of Fallot patients. Global deletion of delta SET domain region of Kmt2c gene that harbour methyltransferase enzymatic activity resulted in neonatal lethality in mice. Histological analysis of knockout mice embryonic heart revealed ventricular septal defect (with and without an overriding aorta) with a low penetrance but also displayed a consistent phenotype resembling ventricular non-compaction. Embryonic hearts from the knockout mice at the e16.5 stage of development displayed a significantly thinner ( $p < 0.05$ ) compact myocardium of the left ventricle compared to the wild-type littermates. In order to get insights into the molecular mechanism for this phenotype, we carried out RNA sequencing experiments in ventricles of e16.5 embryonic hearts from mice with a homozygous deletion and wild type littermates. A significant decrease in gene expression is observed in many of the extracellular matrix (ECM) genes, especially elastin ( $p < 1.0E-6$ ), various subtypes of collagens, fibronectin, and integrins. We also found an altered expression of genes important for ECM homeostasis, e.g. MMPs, and ventricular trabeculation/compaction, e.g. Notch1. ECM is known to play important role in heart development, including trabeculation and formation of compacted myocardium. Our data suggest an important role played by Kmt2c in regulating ECM homeostasis and the formation of compacted myocardium.

## BS27 ECHOCARDIOGRAPHIC EVALUATION OF LEFT VENTRICULAR FUNCTION AND MYOCARDIAL DEFORMATION IN A REPERFUSED MOUSE MODEL OF MYOCARDIAL INFARCTION

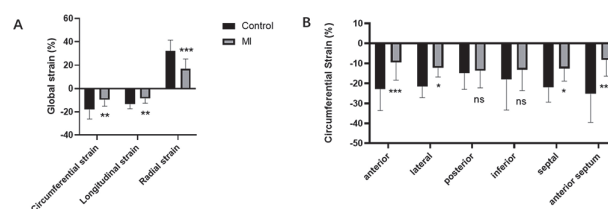
Zhiping Feng. UCL, Paul O'Gorman Building, 72 Huntley Street, Finchley, London, LND WC1E 6DD UK

10.1136/heartjnl-2022-BCS.207

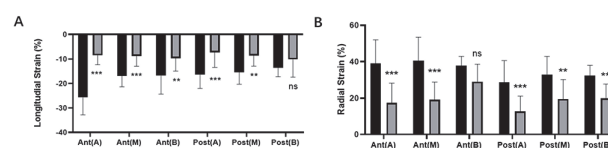
We evaluated the feasibility and accuracy of four-dimensional preclinical ultrasound (4D-US) and speckle-tracking imaging (STI) for monitoring changes in function post reperfused myocardial infarction (MI).

**Methods** Seventeen female mice (age = 10–12 wk) underwent ligation of the left anterior descending coronary artery. Cardiac MRI (Varian 9.4T) and echocardiographic images (Visualsonics 3100) were acquired at 2 weeks ( $n=6$ ) or 8 weeks ( $n=11$ ) post-surgery. Ejection fraction was calculated and then compared between 4D-US, MRI, M-mode and Simpson's multi slice at each time point. Eight healthy mice and seventeen MI mice were used for STI strain analysis.

**Results** All ultrasound methods calculated ejection fractions that correlated with MRI. However, 4D-US provided the strongest agreement, outperforming M-mode and Simpson's multi slice (4D-US:  $R^2 = 0.81$ , M-mode:  $R^2 = 0.55$ , Simpson's:  $R^2 = 0.73$ ) (table 1). STI-derived measures of global strain were significantly lower in the MI group in all dimensions ( $P < 0.005$ ). (Figure 1 A) For regional strain analysis, circumferential strain values in MI were significantly lower in antero-lateral and septal regions compared with control mice ( $P < 0.001$ ). (Figure 1 B). The longitudinal strain and radial



**Abstract BS27 Figure 1** A, Differences in global strain between MI and control groups. B, Differences in regional strain in circumferential between MI and control groups. ns: not statistically significant; \* $P < 0.05$  \*\* $P < 0.005$ , \*\*\* $P < 0.001$ .



**Abstract BS27 Figure 2** A-B, Differences in regional strain in longitudinal and radial between MI and control. Ant(A), anterior apical; Ant(M), anterior mid; Ant(B), anterior basal; Post(A), posterior apical; Post(M), posterior mid; Post(B), posterior basal. ns: not statistically significant; \*\* $P < 0.005$ , \*\*\* $P < 0.0001$ .